CARDIFF UNIVERSITY
PRIFYSGOL CAERDYDD

ORCA – Online Research @ Cardiff

This is an Open Access document downloaded from ORCA, Cardiff University's institutional repository:https://orca.cardiff.ac.uk/id/eprint/129525/

This is the author's version of a work that was submitted to / accepted for publication.

Citation for final published version:

Cho, Yuljae, Hou, Bo , Lim, Jongchul, Lee, Sanghyo, Pak, Sangyeon, Hong, John, Giraud, Paul, Jang, A-Rang, Lee, Young-Woo, Lee, Juwon, Jang, Jae Eun, Snaith, Henry J., Morris, Stephen M., Sohn, Jung Inn, Cha, SeungNam and Kim, Jong Min 2018. Balancing charge carriertransport in a quantum dot P-N junction toward hysteresis-free high-performance solar cells. ACS Energy Letters 3 (4) , pp. 1036-1043. 10.1021/acsenergylett.8b00130

Publishers page: http://dx.doi.org/10.1021/acsenergylett.8b00130

Please note:
Changes made as a result of publishing processes such as copy-editing, formatting and page numbers may not be reflected in this version. For the definitive version of this publication, please refer to the published source. You are advised to consult the publisher's version if you wish to cite this paper.

This version is being made available in accordance with publisher policies. See http://orca.cf.ac.uk/policies.html for usage policies. Copyright and moral rights for publications made available in ORCA are retained by the copyright holders.

Balancing Charge Carrier Transport in a Quantum Dot P–N Junction toward Hysteresis-Free High-Performance Solar Cells

Yuljae Cho,[a,‡] Bo Hou,[a,‡] Jongchul Lim,[b] Sanghyo Lee,[a] Sangyeon Pak,[a] John Hong,[a] Paul Giraud,[a] A-Rang Jang,[a] Young-Woo Lee,[a,c] Juwon Lee,[a] Jae Eun Jang,[d] Henry J. Snaith,[b] Stephen M. Morris,[a] Jung Inn Sohn,[a,e,] SeungNam Cha,[a,*] Jong Min Kim[f]*

[a]*Department of Engineering Science, University of Oxford, Parks Road, Oxford OX1 3PJ, United Kingdom*

[b]*Department of Physics, Clarendon Laboratory, Parks Road, University of Oxford, Oxford OX1 3PU, United Kingdom*

[c]*Department of Energy Systems, Soonchunhyang University, Asan, Chungcheongnamdo, 31538, Republic of Korea*

[d]*Department of Information and Communication Engineering, Daegu Gyeongbuk Institute of Science and Technology, Daegu 711-873, Republic of Korea*

[e]*Division of Physics and Semiconductor Science, Dongguk University, Seoul 100-715, Republic of Korea*

[f]*Department of Engineering, University of Cambridge, 9 JJ Thomson Avenue, Cambridge CB3 0FA, United Kingdom*

ABSTRACT. In a quantum dot solar cell (QDSC) that has an inverted structure, the QD layers form two different junctions between the electron transport layer (ETL) and the other semiconducting QD layer. Recent work on an inverted-structure QDSC has revealed that the junction between the QD layers is the dominant junction, rather than the junction between the ETL and the QD layers, which is in contrast to the conventional wisdom. However, to date, there have been a lack of systematic studies on the role and importance of the QD heterojunction structure on the behavior of the solar cell and the resulting device performance. In this study, we have systematically controlled the structure of the QD junction to balance charge transport, which demonstrates that the position of the junction has a significant effect on the hysteresis effect, fill factor and solar cell performance and is attributed to balanced charge transport.

Table of Content (TOC) graphic

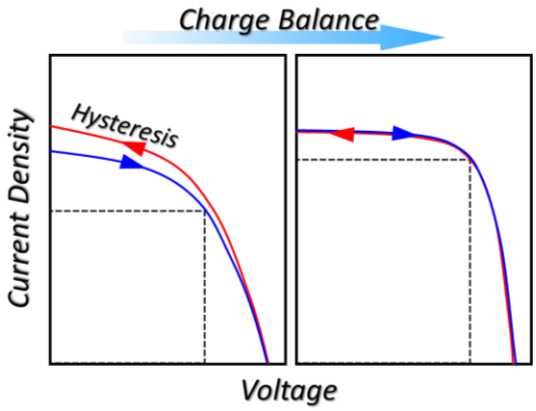

Harvesting photon energy has attracted tremendous interest because it is an environmentally-friendly solution to the global energy demands in response to the exhaustion of fossil fuels.[1,2] In accordance with the development of advanced materials for photon energy harvesting, the field of solar cells has continued to make steady technological progress.[3] In particular, colloidal quantum dots (CQDs) have been shown to be one of the more promising materials for solar cell technology due to the facile and cost-effective synthesis process as well as the extensive tunability of the bandgap.[4-6] Amongst the various CQDs that have been developed, lead-based QDs such as lead sulfide (PbS) have been considered as the most attractive CQDs for photon harvesting devices since they exhibit a large Bohr radius (a = 20 nm), wide bandgap tuning range (E_g = 0.4 to 3.0 eV), and large light absorption coefficients.[6-8] Consequently, rapid progress in the area of PbS quantum dots solar cells (QDSCs) has been made over the past decade.[5-8]

For a PbS QDSC, the most common architecture consists of the following arrangement: electron transport layer (ETL) / n-type QD layers / p-type QD layers.[9-18] Among the various strategies that have been developed to improve the performance of QDSCs, tailoring of the junction interfaces between an electron transport layer (ETL) and the PbS QD layers, as well as between the n-type and p-type QD layers have been found to be crucial for high performance QDSCs.[9-18] However, there are different viewpoints in the literature about which junction plays the dominant role in the efficient transport and collection of the photo-generated charges. A very recent study has revealed that the junction formed between the n- and p-type QD layers is the dominant junction rather than the junction between the ETL and QD layers as it was previously believed.[19] In spite of the recent finding, there is still lack of understanding of the behavior of the charge carriers in accordance with the QD junction architecture. Therefore, further investigation

of the role of the QD p-n junction from a device operation point of view is highly desirable because the QD junction directly influences the behavior of the photo-generated charge transport, the formation of detrimental space charges, hysteresis characteristics and ultimately the QDSC performance.

In this report, we have systematically controlled the structure of the QD p-n junction in PbS QDSCs by manipulating the ratio of the number of n-type QD (tetrabutylammonium iodide (TBAI)) layers to the number of p-type (1,2-ethanedithiol (EDT)) QD layers so as to investigate the correlation between the location of the junction and the corresponding charge transport behavior. Towards this end, the photoelectronic and electrical properties of n- and p-type QD film are analyzed to better understand the behavior of the charge transport in a QD junction, which provides a design motif for the ideal junction structure. Following analysis of the characteristics of the QD films, we demonstrate that the junction structure has a significant effect on the resulting solar cell performance, such as the fill factor (FF) and power conversion efficiency (PCE), which is attributed to balanced charge transport from the QD layers to the electrodes. By controlling the optimal charge balancing point through a structural modification to the QD junction, a higher FF (greater than 70 %), reduced hysteresis and consequently a significantly enhanced PCE (~9%) are achieved. We believe that this enhancement in efficiency is due to a balance of the charges at the QD p-n junction, which suppresses the formation of space charges that can arise through an imbalance in the charge carrier transport.[20,21] In contrast, we observe severe hysteresis, low FF and consequently a decrease in the PCE in QDSCs when the charge transport is not balanced, which occurs due to the formation of space charges and high series resistances.[20,21] In addition, we demonstrate a significant improvement in power generation when comparing two types of solar

modules that consist of a series of QDSCs that are either charge imbalanced or balanced, and we attribute the improved power generation to improved characteristics regarding the internal resistances (low R_s and high R_{sh}) for the latter type of solar cells.

For the fabrication of the PbS QDSCs, PbS QDs were first synthesized and purified according to the processes described in our previous work.[6,8] Further details of the fabrication process and thickness of each layer are provided in the Methods section. Supplementary Figure S1 shows a schematic of a QDSC structure where the labels TBAI and EDT indicate the different types of ligands that were used in the PbS QD layers; these have been the most frequently employed ligands as they exhibit good stability and high PCE amongst the types of QD ligands that have been studied to date.[9-14] The as-prepared colloidal PbS QDs in toluene at a concentration of 50 $mgml^{-1}$ are shown in the inset of Figure 1(a) and it was found that the bandgap was 1.26 eV from measurements of the absorption spectrum of the QD solution using an ultraviolet-visible spectrometer (UV-Vis) as shown in Figure 1(a). A solid-state ligand exchange process was applied in order to substitute the insulating oleic acid (OA) ligands that were initially attached to the PbS QDs for the semiconducting TBAI and EDT ligands. Fourier transform infrared spectroscopy (FTIR) measurements revealed a noticeable decrease in the vibration peaks of the $–CH_2$ and –COO bonds as shown in Supplementary Figure S2, indicating the successful removal of the OA from both types of QD films using a solid-state ligand exchange scheme.[15]

Following this, the energy bands for each TBAI- and EDT-treated QD films were measured using ultraviolet photoelectron spectroscopy (UPS). As shown in Figure 1(b), the TBAI- and EDT-treated QD films were identified as being n-type and p-type, respectively, which originates from

the shift of the band-edge by electrostatic forces that are present in the treated ligands.[9,22] Therefore, when EDT-treated QDs are deposited onto TBAI-treated QDs, a QD p-n junction is formed between the separate QD layers. In a typical QDSC structure (Supplementary Figure S1), two junctions are formed between: (i) the zinc oxide (ZnO) ETL and the n-type QD layer, and (ii) the n-type and p-type QD layers.[9,11,19] However, we have considered the latter junction (the QD p-n junction) in more detail in an effort to balance the charge carrier transport because it is the dominant junction in the structure and, moreover, the ZnO layer (50 nm) is considerably thinner than both the n-type and p-type QD layers (total 300 nm).[19] Figure 1(c) depicts the charge transport behavior in a QD p-n junction when the diffusion length of the charge carriers in the n- and p-type materials are similar to one another (which will be discussed in more detail shortly). As shown in Figure 1(c)-left, when either the n- or p-type layer in the junction is larger than the other layer the collection of electrons and holes becomes unbalanced due to differences in the lengths of travel for the charge carriers when they have similar diffusion lengths. As a result, the imbalance in charges results in space charges being formed across the junction, which leads to less efficient charge transport and severe hysteresis in the device characteristics. In contrast, in a charge-balanced system, through the structural modification of the QD p-n junction (Figure 1(c)-right), the formation of space charges is suppressed and thus charge transport and collection are more efficient than a charge-imbalance architecture. Consequently, a significantly enhanced FF and negligible hysteresis in the QDSC are observed, which leads to a concomitant improvement in the solar cell performance.[23-25]

In order to confirm these postulates, we first characterized the photoelectronic and electrical properties of the TBAI- and EDT-treated QD layers as the charge carrier transport in a junction-

structured solar cell primarily depends on the diffusion length of each photo-generated electron and hole.[23,26] To obtain information about the lifetime and mobility of the charge carriers in each QD film, a time-resolved photoluminescence (TRPL) study was carried out alongside measurements of the space-charge limited current (SCLC). The diffusion length was then calculated from these results, which can be expressed as a function of the mobility and lifetime; $L_D = \sqrt{D\tau}\ where\ D = \left({kT}/{q}\right)\mu$ (L_D diffusion length, D diffusion coefficient, τ carrier lifetime in the absence of a quencher, and μ is the mobility).[27-29] As shown in Figure 2(a), the exciton lifetime of each TBAI- and EDT-treated QD film was extracted by fitting the TRPL decay curves with a biexponential decay function. For the TBAI-treated QD-films, this was characterized by two decay times: τ_1 = 8.02 ± 0.13 ns and τ_2 = 57.64 ± 0.38 ns with prefactors A_1 of 1.37 and A_2 of 0.54, respectively, whereas for the EDT-treated QD film the decay times were found to be τ_1 = 8.99 ± 0.09 ns and τ_2 = 54.86 ± 0.49 ns with prefactors A_1 of 1.69 and A_2 of 0.36, respectively.[28] In both cases, the relatively short lifetime of the first exponent (τ_1) is due to a high rate of transition of interparticle charge and energy transfer, which causes a rapid dissociation of the excitons resulting in the suppression of the band gap emission whereas the longer decay time (τ_2) is attributed to carrier recombination.[29] The results of the TRPL measurements suggest that the carrier lifetimes in both films do not differ significantly in terms of timescales.[30]

The J-V curves shown in Figure 2(b) that were obtained from SCLC measurement were fitted using the Mott-Gurney law as described in the Methods section.[31,32] The mobility of each QD film was extracted from the SCLC region (slope = 2).[33,34] The electron mobility of the TBAI-treated QD film (n-type) and the hole mobility of the EDT-treated QD film (p-type) were found to be μ_e = 3.5 × 10^{-2} $cm^2v^{-1}s^{-1}$ and μ_h = 4.4 × 10^{-2} $cm^2v^{-1}s^{-1}$, respectively. As a result, it was found that the

diffusion lengths for the TBAI- and EDT-treated QD layers were comparable as shown in Figure 2(c) (L_D = 72 nm and L_D = 79 nm for the TBAI- and EDT-treated QD films, respectively), which indicates that the distance over which the photo-generated charges are transported in both the n-type and p-type QD layers are equivalent over the same period of time.[35,36]

Lastly, the conductivity in both dark and light conditions was measured in order to investigate the charge transport and collection on each film, which gives information about the product of the mobility and lifetime of the carriers in a film since the conductivity is a function of mobility and steady state charge density. Consistent with the mobility measurements, the EDT-treated QD film generated slightly higher current than that of the TBAI-treated film, in both dark and light illumination conditions as shown in Figure 2(d).

The results (UPS measurement in Figure 1 and Figure 2) indicate that the formation of the QD p-n junction by depositing p-type QD layers onto n-type QD layers have two significant effects on the device performance. First, the energy barrier formed by energy band bending prevents any backflow of electrons.[9] Second, the exact nature of the structure of the p-n junction is a determinant factor in terms of efficient transport and collection of charge carriers. Taking into account these two properties of the QD junction, it was hypothesized that a judicious structural modification of the QD p-n junction to balance charge carrier transport would further enhance the performance of a QDSC as the balanced charge system would suppress the formation of space charges and thus promote efficient transport of the charges.[20,21,23,24]

Based on the results obtained for the diffusion lengths, which show that the charge carriers in both QD films are similar to one another, we have fabricated two different categories of QDSCs with different junction structures: a reference cell (category 1), consisting of thicker n-type layers with thin p-type treated QD layers, which exhibit an imbalance in the charges in the solar cell system and a solar cell (category 2) whereby the charges are balanced, consisting of n- and p-type layers with similar thicknesses (hereafter referred to as a charge-balanced cell). More information about the QDSCs is provided in Table 1. To present comparative behavior of the QDSCs, illustrative data is presented in Figure 3 for a reference cell with a ratio of 8:4 TBAI- to EDT-treated QD layers and for a charge balanced cell with layer ratio of 6:6 TBAI- to EDT-treated QD layers. As shown in Figure 3(a), a prominent hysteresis and lower FF (57 %) were observed for the reference cell. In contrast, negligible hysteresis and a higher FF (72 %) were obtained for the charge balanced cell (the measured solar cell parameters are shown in Supplementary Table S2), which is attributed to an efficient transport of the charge carriers due to a suppression of the formation of the space charges. In addition, hysteresis in the device characteristics in the reference cell was observed throughout the full J-V scanning range (-0.5 ~ 1 V) whereas a charge balanced cell exhibited negligible hysteresis over the same voltage range. Considering that the contact electrodes for both types of QDSCs (ITO/ZnO/TBAI/EDT/Au) were identical, the results indicate that the hysteresis observed in the reference cell resulted from the formation of space charges not by other external causes, such as charge injection from the electrodes. These collective results indicate that balancing charges by adjusting the structure of the QD p-n junction is necessary to realize hysteresis-free and high FF QDSCs.[20,21,23,24]

Figure 3(b) presents the external quantum efficiency (EQE) of both the reference and charge-balanced QDSCs. By integrating over the EQE curves it was revealed that the J_{sc} of the QDSCs was found to be 19.06 $mAcm^{-2}$ and 20.53 $mAcm^{-2}$ for the reference and charge-balanced cell, respectively, which shows that the J_{sc} has been increased by 1.5 $mAcm^{-2}$ due to the balancing of charges. The improvement in the EQE at longer wavelengths in the charge-balanced cell (shaded in green) is related to the change in the behavior of photo-generated charge transport. As long-wavelength photons are absorbed deeper in the film due to their deeper penetration depths, the EQE result indicates that charges generated by long-wavelength photons were more efficiently transported and collected at the electrodes in spite of their greater distance of travel, which is attributed to the absence of space-charges in the charge-balanced cell.[9] Additionally, the large J_{sc} mismatch that was observed in the reference cell between the J-V and the EQE measurements suggests that the magnitude of the hysteresis in the reference cell is detrimental and limits accurate measurement of the photo-current using a J-V sweep method. In contrast, only a slight discrepancy in J_{sc} was noted between the values obtained from the EQE curves when compared to the J-V sweep measurements for the charge-balanced cell. This is believed to be result of a balanced transport of charge carriers in a junction-structured QDSC.[37-39] However, it is worth noting that, in both cases, a slight mismatch in the measured value of J_{sc} using a J-V sweep and EQE measurement could be associated with a change in the photo-active materials under light illumination and/or measurement error.[12] Lastly, the charge-balanced cells exhibited stable performances when they were stored in ambient air without the need for any encapsulation layer for up to 150 days as shown in Figure 3(c). The result indicates that the insulating OA ligands were successfully removed from the QD surfaces and that the QDs were sufficiently passivated by both ligands, which protects the QD layers from exposure to oxygen.[40]

The results revealed that the configuration of the QD p-n junction plays a significant role in balancing charges in the inverted QDSC structure. Charge balance facilitates the suppression of space charge build-up as well as efficient transport and collection of charge carriers, which results in significantly improved FF and a concomitant enhancement in PCE. It is worth noting that a previous study on the TBAI and EDT junction focused on the role of the EDT as an electron blocking layer (EBL).[9] We further expanded the role of the EDT as a dominant hole transport layer to accomplish charge balance in the QD p-n junction, in addition to its role as an EBL.

Further details about the effect of charge balancing in the QDSCs system are illustrated in Figure 4(a), demonstrating that the FF was continuously improved as the thickness of the EDT-treated QD layer became thicker until the charge balance in the QDSC approached the optimum conditions (6 layers for each of the TBAI- and EDT-treated QDs as the diffusion lengths of charge carriers are similar one another) while the total thickness of the QD layers were maintained at approximately 300 nm. A significant enhancement in FF (Δ27 %, from 55 % to 70 % in average) led to a concomitant improvement in the solar cell performance. Further details of the QDSCs with a different number of TBAI- and EDT-treated QD layers are shown in Table 1. The values were averaged across 30 different QDSC devices. It is worth commenting that the similar J_{sc} levels (slight improvement) observed for the reference and charge-balanced cells are considered to be due to the total thickness of the device being fixed at approximately 300 nm, which is in good agreement with previous reports on charge balancing in perovskite-based solar cells.[23,24]

The charge-balance scheme proposed here also appeared to contribute to the suppression of non-radiative recombination due to the effective transport of the photo-generated charges, which is another indication that the FF has been enhanced.[20,21,23,24] By plotting the photocurrent of the QDSCs as a function of the light intensity on a double logarithmic scale, it was possible to fit the data with a linear function (see Supplementary Figure S3). The extracted power factor α ($I_{sc} \propto I^{\alpha}$, where I_{sc} is the short circuit current and I is the light intensity) provides information about the charge recombination as a loss mechanism for the photocurrent. A power factor, α, close to unity indicates that the photocurrent is determined by the generation rate of the electron-hole pairs under light illumination whereas a value that deviates from unity suggests that the photocurrent is further limited by the formation of space charge regions as a result of the mismatch in the transport of the photo-generated charges.[41,42] For the QDSCs with an equal number of n-type and p-type QD layers, the power factor, α, was found to be close to unity as the charge carriers were balanced across the junction as shown in Figure 4(b). The different values of α for devices with a different ratio of n-type to p-type layers are shown in Table S1.

To further support that balancing charges in a QD junction is an important approach in the development of high performance QDSC devices, we have applied this design criterion to other types of halide ligands, in particular Br (tetrabutylammonium bromide (TBAB)) and Cl (tetrabutylammonium chloride (TBAC)). As shown in Supplementary Figures S4, S5 as well as Tables S2 and S3, a significant increase in the FF and a measurable enhancement in the PCE were observed for devices consisting of other halide ligands with an equal number of layers.

Lastly, the proposed charge-balance scheme was revealed to be of prime importance in a solar module application for the practical application of QDSCs. Studies on a solar module application were performed using the MATLAB/Simulink software by comparing reference cells arranged in a series connection with that of charge balanced cells arranged in the same configuration. More details about the simulation and an equivalent circuit diagram for the solar module are provided in the Supplementary Information and Supplementary Figure S6. As the number of cells connected in series were increased a more prominent effect of the charge-balance scheme in a QDSC was observed as shown in Figures 4(c) and (d). As a result of the higher R_s value that arises from space charges in the reference cells, an undesirable solar panel performance was observed when reference cells were connected in series. For example, it was found that a 29 % and 61 % decrease in the PCE was observed for modules with 5 and 10 reference cells connected in series, respectively. On the contrary, there was a much smaller decrease in the PCE (24 % and 47 % for 5 and 10 cells connected in series, respectively) in charge balanced cells, which was attributed to the lower R_s and higher R_{sh}. Finally, a solar panel that consisted of 50 cells in series and 25 cells in parallel, as an example, showed a huge contrast in terms of the power generation from the solar panels, which was 9.2 W for the panel using charge balanced cells as oppose to 6.8 W for the solar panel that employed the reference cells, as shown in Supplementary Figure S7. These results further demonstrate the importance of a charge-balance scheme and its importance for solar module applications using PbS QDs.

In summary, we have considered the fundamental role of the architecture of the QD p-n junction in the inverted QDSC structure ($ZnO(n^+)$ / QD(n) / QD(p)), which is the most frequently studied device configuration adopted in PbS QDSCs. By measuring the carrier lifetime and

mobility of the TBAI- and EDT-treated QD films, the diffusion lengths of the corresponding films were found to be comparable to one another. Based on the photoelectric characteristics obtained from both QD films, we have devised a p-n junction arrangement in order to balance charge carrier transport. A balanced QDSC exhibited negligible hysteresis, significantly enhanced FF (> 70 %), and concomitant PCE (> 9 %) improvement, which is attributed to the suppression of space charges as well as efficient transport and collection of the photo-generated charges. In contrast, charge imbalance in the system leads to the formation of space charges, which resulted in a notable hysteresis in the J-V curves, low FF, and corresponding poor solar cell performance. Furthermore, a charge balance scheme was applied to other types of halide ligands, notably Br and Cl, which also showed significantly improved FF and PCE compared to QDSCs where the charge carrier transport was not balanced. Lastly, the importance of the charge balance strategy was further supported in simulations of a solar module application for future PbS QDSC technology.

METHODS

Solar cell fabrication method. Colloidal PbS QDs and ZnO nanoparticles in a solution phase were synthesized according to a method that we have described elsewhere.[6,8] A solution of ZnO nanoparticles in chloroform was spin-coated onto patterned ITO (thickness 150 nm) glass substrates (thickness 1.1 mm) at 3000 rpm for 30 seconds. The thickness of the ZnO layer was approximately 50 nm. Subsequently, one drop of PbS QDs solution was spin-coated at 3000 rpm. For the solid-state ligand exchange, a tetrabutylammonium iodide (TBAI) solution in methanol with a concentration of 10 $mgml^{-1}$ was loaded on a PbS QD layer and held for 30 seconds, which was followed by a washing process using methanol that was carried out twice. For halide Br and Cl treatment, 10 $mgml^{-1}$ of tetrabutylammonium bromide (TBAB) and 20 $mgml^{-1}$ of tetrabutylammonium chloride (TBAC) in methanol were used, which was followed by the same washing process. All other conditions were the same unless specified otherwise. 1,2-Ethanedithiol (EDT, 0.02 vol% in acetonitrile) was treated by using a direct coating method without a loading time, followed by a washing process using acetonitrile, which was performed twice. The thickness of each TBAI- and EDT-treated QD layer was controlled by the number of layers deposited and the thickness was fixed at approximately 300 nm for all devices where the thickness of a single layer of either the TBAI- or EDT-treated QD film were almost identical at 24 and 25 nm, respectively. Gold electrodes with 100 nm thickness were deposited using thermal evaporation under a high vacuum.

Solar cell characterization method. Solar cell measurements were performed using a source meter (Keithley 4200-SCS) and a solar simulator (LOT-Quantum Design) with an AM 1.5 G filter (100 $mWcm^{-2}$). A standard cell (Rera system) was measured before the solar cell measurements and all measurements were carried out in ambient air. The size of the active area was 0.03 ± 0.002

cm^2. For light intensity-dependent measurements, a neutral-density (ND) filter was used to control the light intensity incident on the devices.

SCLC devices. Electron and hole-only devices were fabricated using the same method as the QDSCs. The structure of the electron-only device was ITO/ZnO/QD-TBAI/ZnO/Al whereas the structure of the hole-only device was ITO/PEDOT:PSS/TFB/QD-EDT/TFB/Au where TFB is an abbreviation of the compound poly(9,9-dioctylfluorene-alt-N-(4-sec-butylphenyl)-diphenylamine). Measured I-V curves were fitted using the Mott-Gurney law, $J_D = \frac{9\varepsilon\varepsilon_0\mu V_b^2}{8D^3}$, where V_b is the applied voltage and D the total thickness of the device as described in Refs. 32 and 35. For the calculation of the mobility, we used a value of 21.2 for the dielectric constant of the PbS QDs as reported in Ref. 14. The total thickness of the electron-only device and the hole-only device were 400 and 375 nm, respectively.

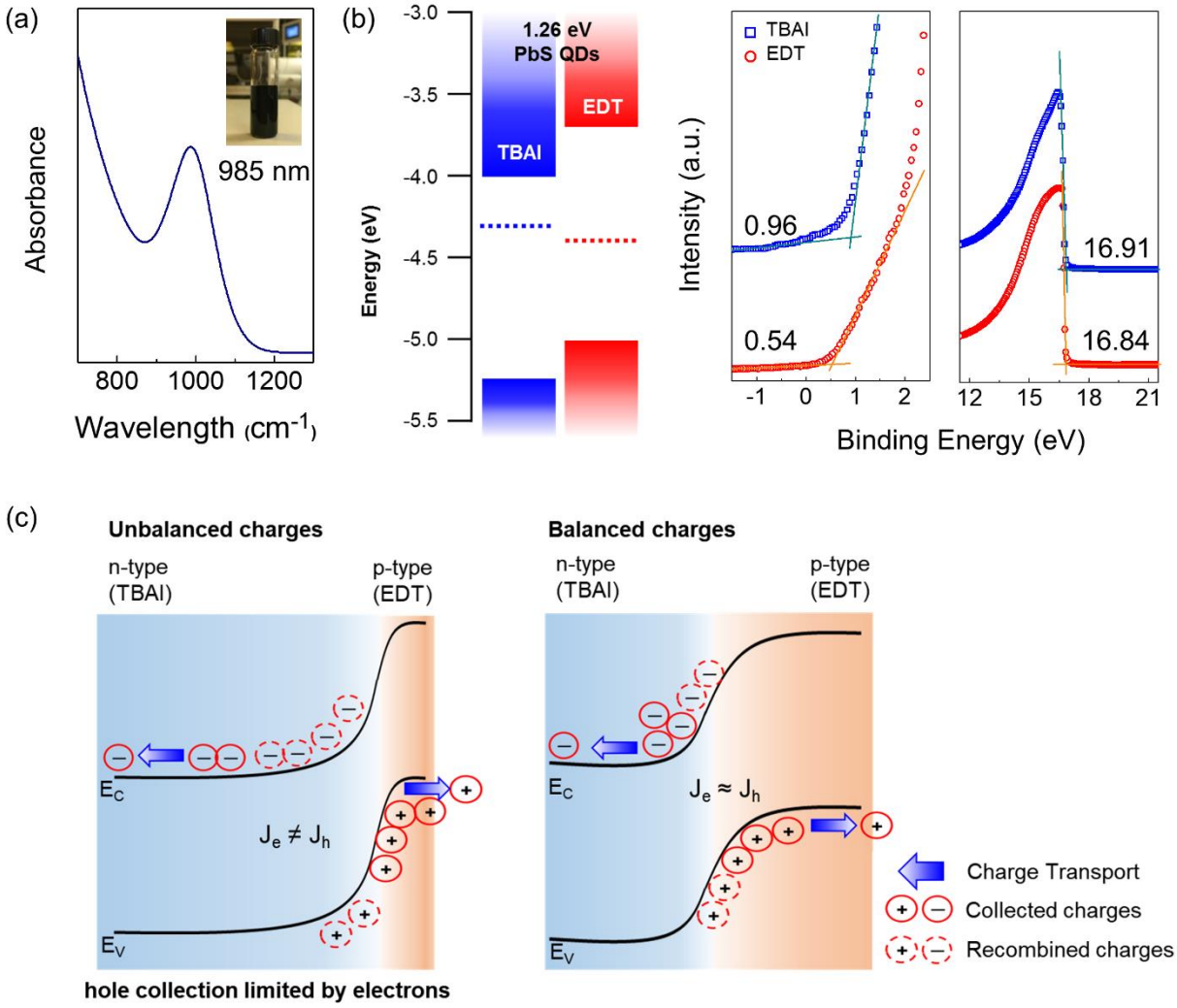

Figure 1. (a) The absorption spectrum of the as-synthesized PbS QDs measured using UV-Vis spectroscopy (inset: a photograph of the QDs in a solution of toluene). (b) Energy levels of the TBAI- and EDT-treated QD films (left diagram) and the results obtained from UPS measurements (right plots). (c) A two-dimensional illustration of the charge carrier balance scheme in a typical p-n junction structured solar cell when the lifetime and mobility of the charge carriers in the n-type layers and p-type layers are equivalent. J_e and J_h denote the electron and hole current densities, respectively.

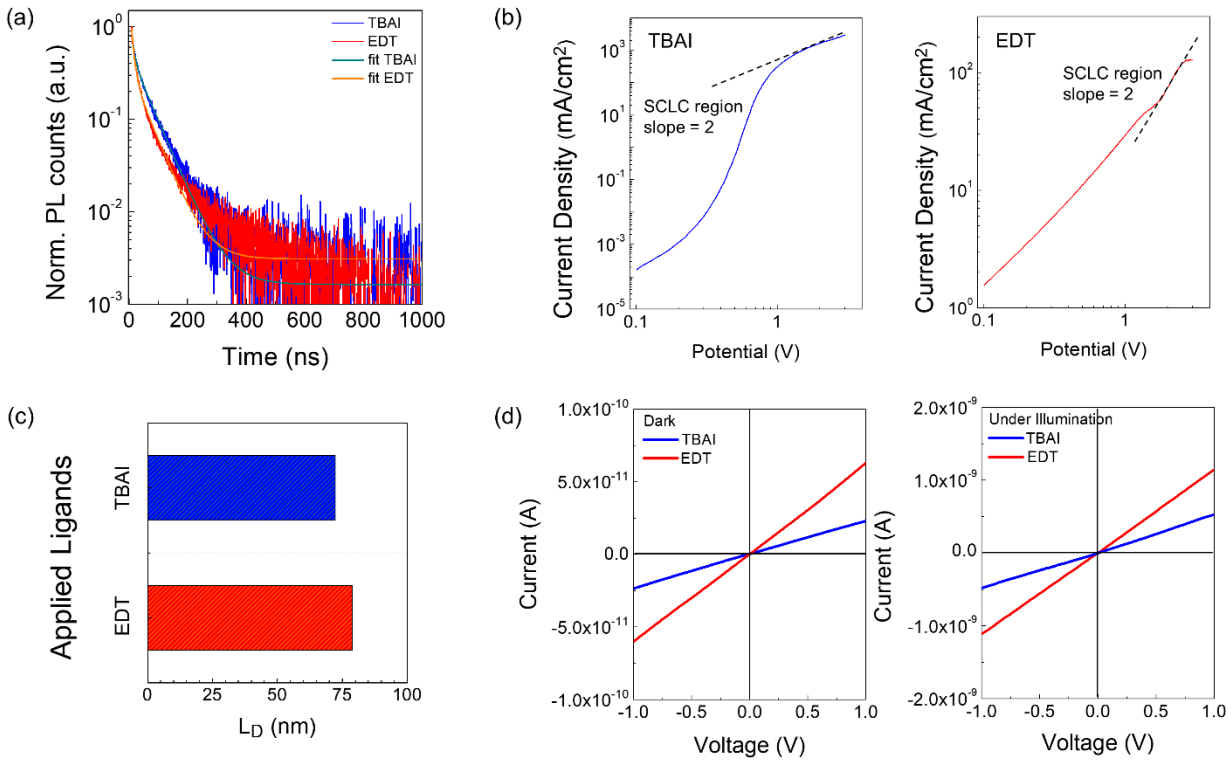

Figure 2. (a) Time resolved photoluminescence of the TBAI- and EDT- passivated PbS QDs films. (b) Current-voltage curves for an electron-only (TBAI) (left plot) and a hole-only (EDT) (right plot) device. The mobility of each layer was extracted from the SCLC region (slope = 2). (c) Calculated diffusion lengths of the charge carriers in the QD film treated with either TBAI (Blue) or EDT ligands (Red). (d) Conductivity measurements of the TBAI- (Blue) and EDT-treated (Red) films carried out in dark conditions and under illumination (white light).

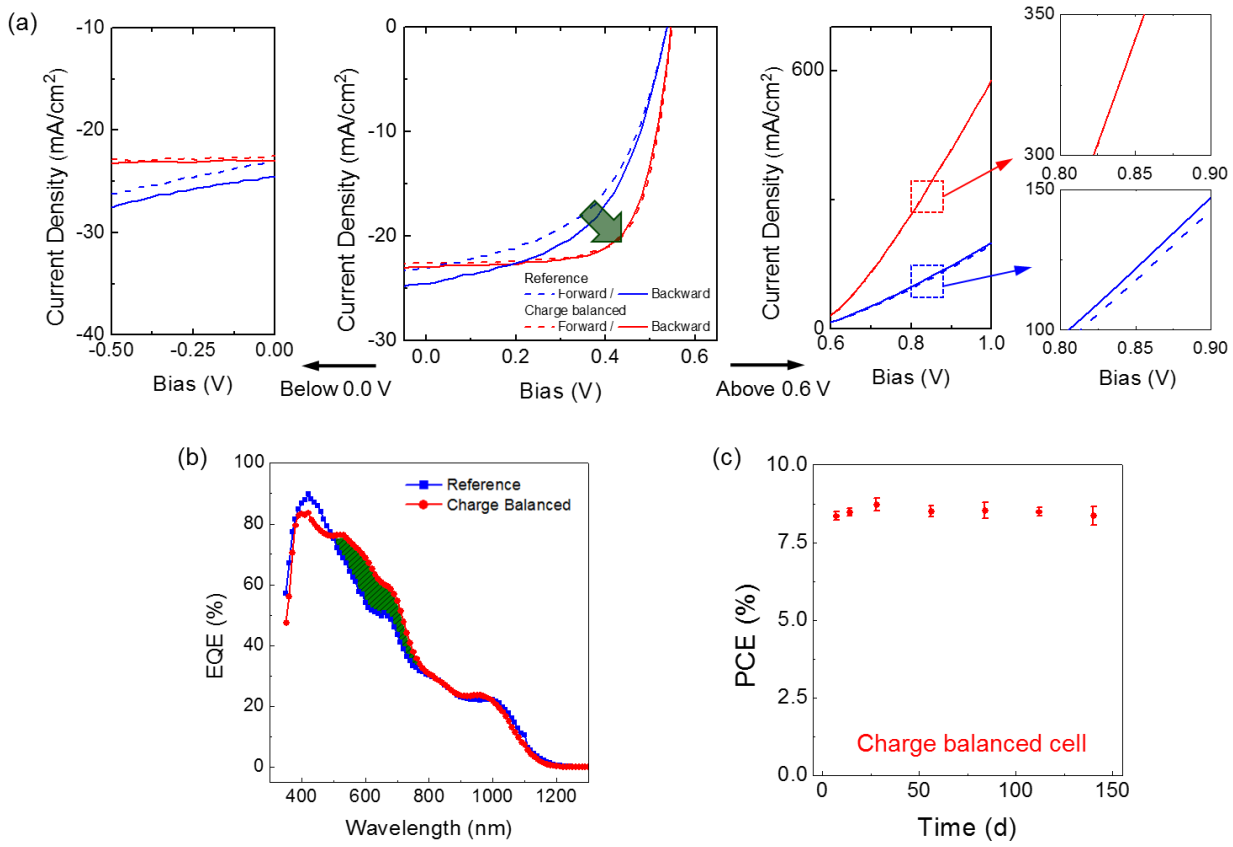

Figure 3. (a) J–V characteristics of the reference (blue) and the charge balanced cell (red) with respect to the bias voltage range (–0.5 ~ 0, 0 ~ 0.6, and 0.6 ~ 1 V) where the dotted lines correspond to a forward sweep of the bias voltage and the solid lines correspond to a reverse sweep in the bias voltage. (b) EQE curves for the reference cell and for the charge-balanced cell. (c) Power conversion efficiencies of the charge-balanced cells stored in ambient air, which was measured periodically over a period of almost 150 days.

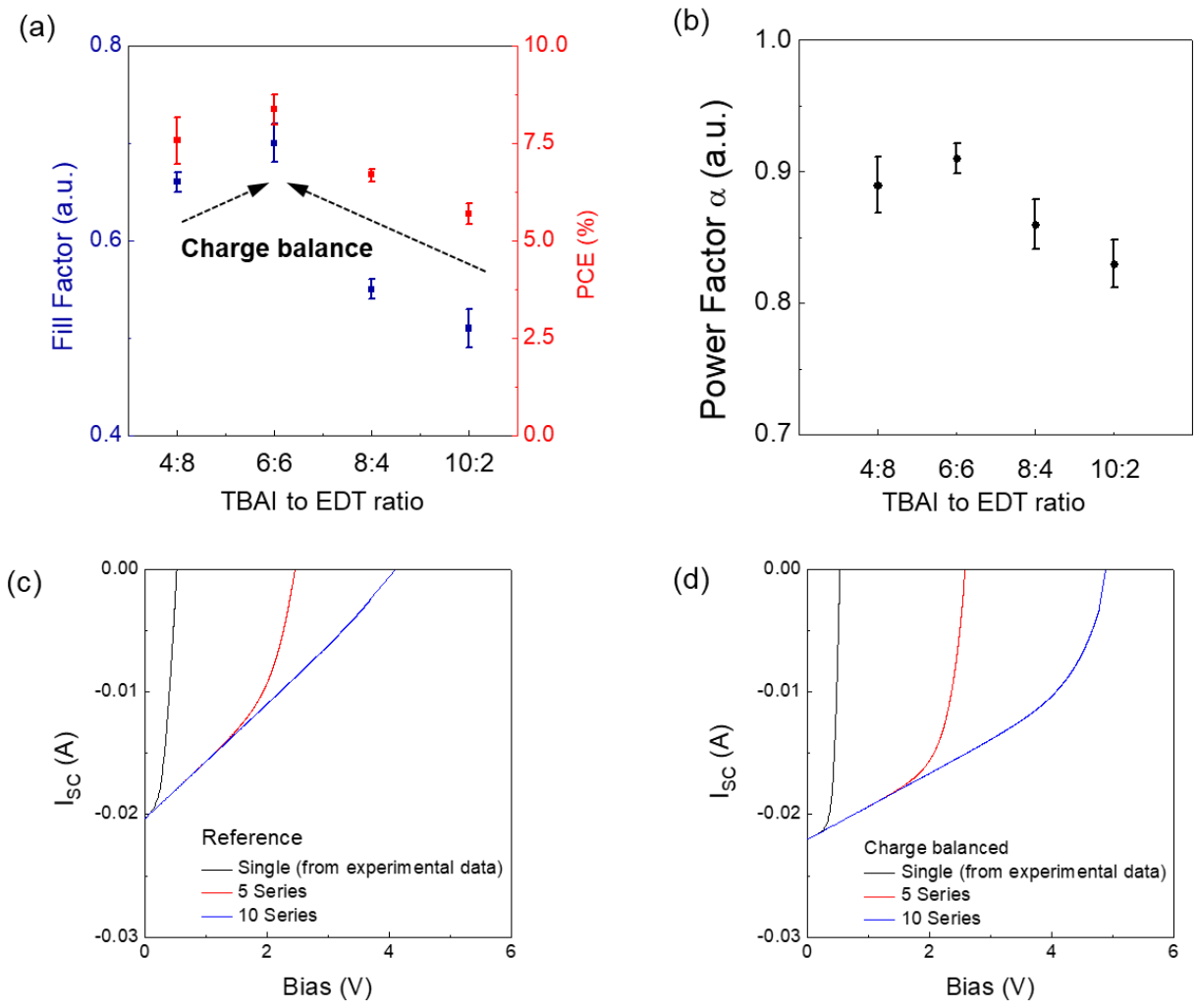

Figure 4. (a) Changes in the solar cell fill factor and performance conversion efficiency with respect to the different number of TBAI- and EDT-treated QD layers in the QDSCs. (b) Light intensity-dependent short circuit current measurement of QDSCs. Simulation results for (c) the reference and (d) charge-balanced cells connected in series for a solar module application.

Table 1. Average solar cell parameters of the TBAI-EDT QDSCs with respect to the different number of layers in the TBAI- to EDT-treated QDs. J_{sc} extracted from the EQE spectra are quoted in the parentheses.

Device Category	Number of layers TBAI:EDT	V_{oc} (V)	J_{sc} (mAcm^{-2})	R_s (Ωcm^2)	R_{sh} (Ωcm^2)	FF	PCE (%)
Category 2 (Charge balanced) ↑	6:6	0.54 ± 0.01	22.38 ± 1.47 (20.53)	2.11 ± 0.79	368.54 ± 39.83	0.70 ± 0.02	8.36 ± 0.38
	4:8	0.54 ± 0.01	21.36 ± 1.83 (18.66)	2.51 ± 1.14	341.99 ± 33.82	0.66 ± 0.01	7.57 ± 0.60
Category 1 (Charge unbalanced)	8:4	0.54 ± 0.01	22.10 ± 1.75 (19.06)	7.70 ± 1.81	252.61 ± 16.37	0.55 ± 0.01	6.68 ± 0.16
	10:2	0.53 ± 0.01	21.21 ± 1.50 (18.09)	8.82 ± 0.56	205.43 ± 12.73	0.51 ± 0.02	5.68 ± 0.26

ASSOCIATED CONTENT

Supporting Information

Structure of a QDSC, FTIR measurement, light intensity-dependent solar cell performance, performances of QDSCs with different types of halide ligands, and MATLAB/Simulink simulation result in Figures S1−S8 and Tables S1−S3 (PDF).

AUTHOR INFORMATION

Corresponding Author

*E-mail: junginn.sohn@dongguk.edu,

*E-mail: seungnam.cha@eng.ox.ac.uk.

ORCID

Yuljae Cho: 0000-0003-2976-0604

Bo Hou: 0000-0001-9918-8223

Sangyeon Pak: 0000-0003-1765-3043

John Hong: 0000-0002-1513-8622

Jung Inn Sohn: 0000-0002-3155-4327

SeungNam Cha: 0000-0001-6284-8312

Author Contributions

‡Y. C. and B. H. contributed equally to this work.

Notes

The authors declare no competing financial interest

ACKNOWLEDGMENT

This work was supported by the National Research Foundation of Korea (NRF) (2015M2A2A6A02045252), and the European Research Council under ERC Grant Agreement number 340538 and the European Commission Horizon 2020 under grant agreement number 685758.

REFERENCES

(1) Lewis, N. S. Toward Cost-Effective Solar Energy Use. *Science* **2007**, *315*, 798-801.

(2) Sargent, E. H. Colloidal Quantum Dot Solar Cells. *Nat. Photon.* **2012**, *6*, 133-135.

(3) Service, R. F. Solar Energy. Can the Upstarts Top Silicon? *Science* **2008**, *319*, 718-720.

(4) Kim, J. Y.; Voznyy, O.; Zhitomirsky, D.; Sargent, E. H. 25th Anniversary Article: Colloidal Quantum Dot Materials and Devices: A Quarter-Century of Advances. *Adv. Mater.* **2013**, *25*, 4986-5010.

(5) Cao, Y.; Stavrinadis, A.; Lasanta, T.; So, D.; Konstantatos, G. The Role of Surface Passivation for Efficient and Photostable PbS Quantum Dot Solar Cells. *Nat. Energy* **2016**, *1*, 16035.

(6) Hou, B.; Cho, Y.; Kim, B. S.; Hong, J.; Park, J. B.; Ahn, S. J.; Sohn, J. I.; Cha, S.; Kim, J. M. Highly Monodispersed PbS Quantum Dots for Outstanding Cascaded-Junction Solar Cells. *ACS Energy Lett.* **2016**, *1*, 834-839.

(7) Michalet, X.; Pinaud, F. F.; Bentolila, L. A.; Tsay, J. M.; Doose, S.; Li, J. J.; Sundaresan, G.; Wu, A. M.; Gambhir, S. S.; Weiss, S. Quantum Dots for Live Cells, in Vivo Imaging, and Diagnostics. *Science* **2005**, *307*, 538-544.

(8) Hou, B.; Cho, Y.; Kim, B. –S.; Ahn, D.; Lee, S.; Park, J. B.; Lee, Y.; Hong, J.; Im, H.; Morris, S. M. *et al.* Red Green Blue Emissive Lead Sulfide Quantum Dots: Heterogeneous Synthesis and Applications. *J. Mater. Chem. C* **2017**, *5*, 3692-3698.

(9) Chuang, C. M.; Brown, P. R.; Bulović, V.; Bawendi, M. G. Improved Performance and Stability in Quantum Dot Solar Cells through Band Alignment Engineering. *Nat. Mater.* **2014**, *13*, 796-801.

(10) Chuang, C. M.; Maurano, A.; Brandt, R. E.; Hwang, G. W.; Jean, J.; Buonassisi, T.; Bulović, V.; Bawendi, M. G. Open-Circuit Voltage Deficit, Radiative Sub-Bandgap States, and Prospects in Quantum Dot Solar Cells. *Nano Lett.* **2015**, *15*, 3286-3294.

(11) Liu, M.; de Arquer, F.; Li, Y.; Lan, X.; Kim, G.; Voznyy, O.; Jagadamma, L. K.; Abbas, A. S.; Hoogland, S.; Lu, Z. *et al.* Double-Sided Junctions Enable High-Performance Colloidal-Quantum-Dot Photovoltaics. *Adv. Mater.* **2016**, *28*, 4142-4148.

(12) Lan, X.; Voznyy, O.; Kiani, A.; Pelayo García de Arquer, F.; Abbas, A. S.; Kim, G.; Liu, M.; Yang, Z.; Walters, G.; Xu, J. *et al.* Passivation Using Molecular Halides Increases Quantum Dot Solar Cell Performance. *Adv. Mater.* **2016**, *28*, 299-304.

(13) Liu, M.; Voznyy, O.; Sabatini, R.; Pelayo García de Arquer, F.; Munir, R.; Balawi, A. H.; Lan, X.; Fan, F.; Walters, G.; Kirmani, A. R. *et al.* Hybrid Organic–Inorganic Inks Flatten the Energy Landscape in Colloidal Quantum Dot Solids. *Nat. Mater.* **2017**, *16*, 258-263.

(14) Aqoma, H.; Al Mubarok, M.; Hadmojo, W. T.; Lee, E.; Kim, T.; Ahn, T. K.; Oh, S.; Jang, S. High-Efficiency Photovoltaic Devices Using Trap-Controlled Quantum-Dot Ink prepared via Phase-Transfer Exchange. *Adv. Mater*. **2017**, *29*, 1605756.

(15) Hong, J.; Hou, B.; Lim, J.; Pak, S.; Kim, B. –S.; Cho, Y.; Lee, J.; Lee, Y.; Giraud, P.; Lee, S. *et al.* Enhanced Charge Carrier Transport Properties in Colloidal Quantum Dot Solar Cells via Organic and Inorganic Hybrid Surface Passivation. *J. Mater. Chem. A* **2016**, *4*, 18769-18775.

(16) Rekemeyer, P. H.; Chang, S.; Chuang, C. M.; Hwang, G. W.; Bawendi, M. G.; Gradečak, S. Enhanced Photocurrent in PbS Quantum Dot Photovoltaics via ZnO Nanowires and Band Alignment Engineering. *Adv. Energy Mater*. **2016**, *6*, 1600848.

(17) Azmi, R.; Oh, S.; Jang, S. High-Efficiency Colloidal Quantum Dot Photovoltaic Devices Using Chemically Modified Heterojunctions. *ACS Energy Lett.* **2016**, *1*, 100-106.

(18) Tang, J.; Liu, H.; Zhitomirsky, D.; Hoogland, S.; Wang, X.; Furukawa, M.; Levina, L.; Sargent, E. H. Quantum Junction Solar Cells. *Nano Lett.* **2012**, *12*, 4889-4894.

(19) Rekemeyer, P.; Chuang, C. M.; Bawendi, M. G.; Gradecak, S. Minority Carrier Transport in Lead Sulfide Quantum Dot Photovoltaics. *Nano Lett.* **2017**, *17*, 6221-6227.

(20) Chiang, C.; Wu, C. Bulk Heterojunction Perovskite–PCBM Solar Cells with High Fill Factor. *Nat. Photon.* **2016**, *10*, 196-200.

(21) Zhou, H.; Chen, Q.; Li, G.; Luo, S.; Song, T. B.; Duan, H. S.; Hong, Z.; You, J.; Liu, Y.; Yang, Y. Interface Engineering of Highly Efficient Perovskite Solar Cells. *Science* **2014**, *345*, 542-546.

(22) Brown, P. R.; Kim, D.; Lunt, R. R.; Zhao, N.; Bawendi, M. G.; Grossman, J. C.; Bulović, V. Energy Level Modification in Lead Sulfide Quantum Dot Thin Films through Ligand Exchange. *ACS Nano* **2014**, *8*, 5863.

(23) Chen, K.; Hu, Q.; Liu, T.; Zhao, L.; Luo, D.; Wu, J.; Zhang, Y.; Zhang, W.; Liu, F.; Russell, T. P. *et al.* Charge-Carrier Balance for Highly Efficient Inverted Planar Heterojunction Perovskite Solar Cells. *Adv. Mater.* **2016**, *28*, 10718-10724.

(24) Heo, J. H.; Han, H. J.; Kim, D.; Ahn, T. K.; Im, S. H. Hysteresis-Less Inverted $CH_3NH_3PbI_3$ Planar Perovskite Hybrid Solar Cells with 18.1% Power Conversion Efficiency. *Energy Environ. Sci.* **2015**, *8*, 1602-1608.

(25) Ponseca Jr, C. S.; Savenije, T. J.; Abdellah, M.; Zheng, K.; Yartsev, A.; Pascher, T.; Harlang, T.; Chabera, P.; Pullerits, T.; Stepanov, A. *et al.* Organometal Halide Perovskite Solar Cell Materials Rationalized: Ultrafast Charge Generation, High and Microsecond-Long Balanced Mobilities, and Slow Recombination. *J. Am. Chem. Soc.* **2014**, *136*, 5189-5192.

(26) Xing, G.; Mathews, N.; Sun, S.; Lim, S.S.; Lam, Y.M.; Grätzel, M.; Mhaisalkar, S.; Sum, T.C. Long-Range Balanced Electron- and Hole-Transport Lengths in Organic-Inorganic $CH_3NH_3PbI_3$. *Science* **2013**, *342*, 344-347.

(27) Parrott, E. S.; Milot, R. L.; Stergiopoulos, T.; Snaith, H. J.; Johnston, M. B.; Herz, L. M. Effect of Structural Phase Transition on Charge-Carrier Lifetimes and Defects in $CH_3NH_3SnI_3$ Perovskite. *J. Phys. Chem. Lett.* **2016**, *7*, 1321-1326.

(28) Sanchez, R. S.; de la Fuente, M. S.; Suarez, I.; Muñoz-Matutano, G.; Martinez-Pastor, J. P.; Mora-Sero, I. Tunable Light Emission by Exciplex State Formation between Hybrid Halide Perovskite and Core/Shell Quantum Dots: Implications in Advanced LEDs and Photovoltaics. *Sci. Adv.* **2016**, *2*, e1501104.

(29) Moroz, P.; Kholmicheva, N.; Mellott, B.; Liyanage, G.; Rijal, U.; Bastola, E.; Huband, K.; Khon, E.; McBride, K.; Zamkov, M. Suppressed Carrier Scattering in CdS-Encapsulated PbS Nanocrystal Films. *ACS Nano* **2013**, *7*, 6964-6977.

(30) Guglietta, G. W.; Diroll, B. T.; Gaulding, E. A.; Fordham, J. L.; Li, S.; Murray, C. B.; Baxter, J. B. Lifetime, Mobility, and Diffusion of Photoexcited Carriers in Ligand-Exchanged Lead Selenide Nanocrystal Films Measured by Time-Resolved Terahertz Spectroscopy. *ACS Nano* **2015**, *9*, 1820-1828.

(31) Dong, Q.; Fang, Y.; Shao, Y.; Mulligan, P.; Qiu, J.; Cao, L.; Huang, J. Electron-Hole Diffusion Lengths > 175 μm in Solution-Grown $CH_3NH_3PbI_3$ Single Crystals. *Science* **2015**, *347*, 967-970.

(32) Guo, X.; Zhou, N.; Lou, S. J.; Smith, J.; Tice, D. B.; Hennek, J. W.; Ortiz, R. P.; Navarrete, J. T. L.; Li, S.; Strzalka, J. *et al.* Polymer Solar Cells with Enhanced Fill Factors. *Nat. Photon.* **2013**, *7*, 825-833.

(33) Li, M.; Li, B.; Cao, G.; Tian, J. Monolithic $MAPbI_3$ Films for High-Efficiency Solar Cells *via* Coordination and a Heat Assisted Process. *J. Mater. Chem. A* **2017**, *5*, 21313-21319.

(34) Yun, D.Y.; Park, H.M.; Kim, S.W.; Kim, S.W.; Kim, T.W. Enhancement of Memory Margins for Stable Organic Bistable Devices Based on Graphene-Oxide Layers due to Embedded $CuInS_2$ Quantum Dots. *Carbon* **2014**, *75*, 244-248.

(35) Zhitomirsky, D.; Voznyy, O.; Levina, L.; Hoogland, S.; Kemp, K. W.; Ip, A. H.; Thon, S. M.; Sargent, E. H. Engineering Colloidal Quantum Dot Solids within and beyond the Mobility-Invariant Regime. *Nat. Commun.* **2014**, *5*, 3803.

(36) Zhitomirsky, D.; Furukawa, M.; Tang, J.; Stadler, P.; Hoogland, S.; Voznyy, O.; Liu, H.; Sargent, E. H. N-Type Colloidal-Quantum-Dot Solids for Photovoltaics. *Adv. Mater.* **2012**, *24*, 6181-6185.

(37) Yang, Z.; Janmohamed, A.; Lan, X.; Pelayo García de Arquer, F.; Voznyy, O.; Yassitepe, E.; Kim, G.; Ning, Z.; Gong, X.; Comin, R. *et al.* Colloidal Quantum Dot Photovoltaics Enhanced by Perovskite Shelling. *Nano Lett.* **2015**, *15*, 7539-7543.

(38) Pradhan, S.; Stavrinadis, A.; Gupta, S.; Christodoulou, S.; Konstantatos, G. Breaking the Open-Circuit Voltage Deficit Floor in PbS Quantum Dot Solar Cells through Synergistic Ligand and Architecture Engineering. *ACS Energy Lett.* **2017**, *2*, 1444-1449.

(39) Stavrinadis, A.; Pradhan, S.; Papagiorgis, P.; Itskos, G.; Konstantatos, G. Suppressing Deep Traps in PbS Colloidal Quantum Dots via Facile Iodide Substitutional Doping for Solar Cells with Efficiency >10%. *ACS Energy Lett.* **2017**, *2*, 739-744.

(40) Ning, Z.; Voznyy, O.; Pan, J.; Hoogland, S.; Adinolfi, V.; Xu, J.; Li, M.; Kirmani, A. R.; Sun, J.; Minor, J. *et al.* Air-Stable n-Type Colloidal Quantum Dot Solids. *Nat. Mater.* **2014**, *13*, 822-828.

(41) Zhao, N.; Osedach, T. P.; Chang, L.; Geyer, S. M.; Wanger, D.; Binda, M. T.; Arango, A. C.; Bawendi, M. G.; Bulovic, V. Colloidal PbS Quantum Dot Solar Cells with High Fill Factor. *ACS Nano* **2010**, *4*, 3743-3752.

(42) Mihailetchi, V.; Wildeman, J.; Blom, P. Space-Charge Limited Photocurrent. *Phys. Rev. Lett.* ***2005***, *94*, 126602.